Yin, T., Zhang, Z., Huang, X., Shire, T. and Hanley, K. J. (2021) On the morphology and pressure-filtration characteristics of filter cake formation: insight from coupled CFD–DEM simulations. *Tunnelling and Underground Space Technology*, 111, 103856.

(doi: 10.1016/j.tust.2021.103856)

Highlights

- Different types of filter cakes were obtained using CFD-DEM coupled simulations
- Slurry infiltration was closely related to the dynamic change of pore structure
- Quantitative correlations were established between pressure drop and pore throat size

On the morphology and pressure-filtration characteristics of filter cake formation: insight from coupled CFD–DEM simulations

Tong Yin [a, b], Zixin Zhang [a, b], Xin Huang [a, b*], Thomas Shire [c], Kevin J. Hanley [d]

[a] Department of Geotechnical Engineering, College of Civil Engineering, Tongji University, Shanghai 200092, P.R. China

[b] Key Laboratory of Geotechnical and Underground Engineering, Ministry of Education, Tongji University, Shanghai 200092, P.R. China

[c] School of Engineering, University of Glasgow, Glasgow, UK

[d] School of Engineering, Institute for Infrastructure and Environment, The University of Edinburgh, Edinburgh EH9 3JL, UK

* Corresponding author at: Department of Geotechnical Engineering, College of Civil Engineering, Tongji University, 1239 Siping Road, Yangpu District, Shanghai 200092, P.R. China.

E-mail address: xhuang@tongji.edu.cn (Xin Huang).

Declaration of interest: none.

Abstract

The slurry filtration process at a tunnel face plays an important role in supporting pressure transmission, which is crucial to the stability of a tunnel face during shield tunneling. In this paper, a series of coupled computational fluid dynamics (CFD)–discrete element method (DEM) numerical simulations were carried out to model the slurry filtration column test. A simplified JKR (Johnson-Kendall-Roberts) model was used to simulate the cohesion between slurry particles. Four types of filter cake formation were identified under different combinations of size ratios between slurry and sand particles, and cohesion between slurry particles according to morphology and pore pressure distribution characteristics. These types were external filter cake, external & internal filter cake, internal filter cake & deep penetration and external & internal filter cake & deep penetration. The contact-based analysis of the constriction (void throat) sizes reveals that the dynamic evolution of the pore structure is closely related to the slurry infiltration process, i.e., the infiltration of slurry particles tends to seal the infiltration channel, which prevents infiltration of any more particles. The variation of D_{c50} (the median constriction size) is closely related to the infiltration state of the slurry particles. The pressure drop within the filter cake becomes significant, i.e., the filter cake will become effective, only when the ratio of D_{c50} to the size of slurry particles is below a threshold value. The current study provides new insight into the fundamental mechanism underlying the slurry filtration process during shield tunneling.

Keywords: Slurry filtration; Coupled CFD–DEM simulation; Morphology; Pressure drop; Pore structure analysis; Constriction size distribution

1. Introduction

The water and soil pressures ahead of a tunnel face during slurry pressure balance (SPB) shield tunneling are supported by pressurized slurry suspensions. During the tunneling process, a filter cake is formed dynamically as the slurry infiltrates into the strata. The quality of filter cake determines the efficiency of support pressure transmission, which controls the tunnel face stability and ground surface settlement. In engineering practice, a filter cake with low porosity and low permeability is favored [1]. However, when tunneling in strata with large pores and high permeability, e.g., sand and gravel, a compact filter cake is difficult to form, leading to insufficient support pressure in front of the tunnel face [2]. Consequently, a thorough understanding of the slurry filtration and filter cake formation in highly permeable ground is important for the safety and economics of SPB tunneling.

A common approach to investigate the slurry filtration process is the slurry filtration column test [3-5]. During the test, a sand column is firstly prepared and saturated in a Perspex cylinder. A certain amount of slurry is poured into the cylinder, which is then pressurized under a constant pressure head on the top, normally using an air pump. The slurry infiltrates into the sand column under the prescribed pressure head and the progressive formation of filter cake can be observed. It has been found that the slurry filtration process and characteristics of filter cake depend on many factors, including shear strength, viscosity and bentonite content of slurry, and the relative size between the sand and slurry particles [6-9]. The last of these has been adopted as a major criterion to characterize the slurry infiltration process and filter cake formation. For example, Min et al. [10] conducted a series of slurry filtration tests and identified three basic types of filter cake depending on the size ratio between sand and slurry particles (see Figure 1). Min et al. chose the characteristic sizes of sand as D_{15}^{sd} (15% by mass is finer than this value) and of slurry particles as d_{85}^{sl} (85% by mass is finer). Based on this, they defined type I as all slurry particles settling on top of the sand column to form a thick layer of filter cake, occurring when $\frac{D_{15}^{sd}}{d_{85}^{sl}} < 5.26$; type II as some slurry particles infiltrating into the sand column and a filter cake plus an infiltration zone are observed, occurring when $5.26 < \frac{D_{15}^{sd}}{d_{85}^{sl}} < 10.53$; and type III, when $\frac{D_{15}^{sd}}{d_{85}^{sl}} > 10.53$, in which most of the slurry particles infiltrate deeply into the sand column forming an infiltration zone without filter cake.

The slurry infiltration process is in essence analogous to the internal erosion in dams. While in the former the small slurry particles fill the pores between large soil particles, in the latter the small particles of base materials are flushed out through the pores of filter particles under a hydraulic gradient. The sand column and slurry particles in slurry filtration column tests are analogous to the filter and clay core materials in dam internal erosion problems, respectively. Terzaghi [11] proposed the classical filtration rule based on experimental results, i.e., an effective filter that can retain the base material should satisfy $D_{15}/d_{85} \leq 4$, where D_{15} is for the filter and d_{85} is for the base material. This filter rule stated, in other words, that when $D_{15}/d_{85} \leq 4$, a compact filter cake could form on the surface of the filter. Bertram [12] and some subsequent studies [13-14] using similar experimental setups or numerical simulations showed that this rule was valid but somehow conservative. Sherard et al. [15] found in their filter tests that base material with d_{85} larger than $0.12D_{15}$ was always retained by the filter and erosion would not happen. Foster and Fell [16] proposed that filter tests could be categorized into three types: (*i*) no erosion (*ii*) some erosion (*iii*) continuing erosion. In the case of slurry filtration, 'no erosion' indicates the formation of compact filter cake, 'some erosion' means that some slurry particles infiltrate into the strata forming an infiltration zone, while others are retained on the surface forming a filter cake, and 'continuing erosion' refers to the case when almost all slurry particles infiltrate deeply into strata without forming a filter cake. They found that D_{15}/d_{85} gave a satisfactory boundary between (*i*) and (*ii*), while D_{15}/d_{95} was more plausible for distinguishing (*ii*) from (*iii*).

So far, there is no consensus about the size ratio criterion for identifying different slurry filtration behaviors. In fact, the pore structure of the sand determines the channel size for slurry particle infiltration. Slurry infiltration can only occur when the characteristic throat size of the sand pores is larger than a certain proportion of slurry particles. Therefore, the size ratio between the pore throats and slurry particles seems to be a more plausible criterion than that between the sand and slurry particles. The dependency of dam internal erosion on the ratio between the characteristic sizes of the filter pore throats and base material has been studied both experimentally [17] and numerically [18,19]. However, no such criterion has been established for slurry filtration problems. Moreover, slurry filtration is a process during which the porosity and pore structure of sand change dynamically, which has not yet been well understood. While the filtration column test is a good way to gain an understanding of macro-filtration behavior, it is difficult to quantify the pore network within the sand column during the tests. Therefore, an alternative approach to study the micro-mechanisms of slurry filtration is desirable.

In this paper, following [20] a series of coupled CFD–DEM numerical simulations of slurry filtration tests were carried out to study the slurry filtration and filter cake formation process during shield tunneling. Different types of slurry filtration behavior were investigated by selecting different combinations of size ratios between slurry and sand particles and cohesion values between slurry particles. The corresponding slurry pressure filtration characteristics, i.e., the porosity and pressure distributions within the filter cake, were used to evaluate the effectiveness of filter cake. Furthermore, the fundamental micro-mechanism underlying each type of slurry filtration phenomenon was explored by analyzing the pore structure of the filter cake based on the constriction size distribution (CSD) obtained by a contact-based void partitioning method [21].

2. Methodology and model implementation

2.1 CFD–DEM Scheme

The coupled CFD–DEM simulations were conducted using three open-source codes: the CFD code OpenFOAM (Open Source Field Operation and Manipulation) (www.openfoam.com), the DEM code LIGGGHTS (LAMMPS improved for general granular and granular heat transfer simulations) [22] and their coupled computation code CFDEM [23]. The major procedure of coupled CFD–DEM simulation follows [20] and is summarized in Figure 2.

The velocities and locations of particles were calculated by Newton's Laws of Motion through LIGGGHTS. The principles of DEM are outlined in [24]. In these simulations, a simplified JKR (Johnson-Kendall-Roberts) model [25] was used for approximating the cohesion forces between slurry particles. If two particles are in contact, an additional normal cohesive force is applied, which is given by [26]:

$$F_{\text{sjkr}} = kA \tag{1}$$

where A is the contact area between particles and k is the cohesion energy density: an empirical parameter. This model has been shown to be appropriate for simulating the cohesive effect of granular materials with low cohesion energy and Young's modulus such as slurry suspensions [20].

The fluid phase is described by the Navier–Stokes equations in Eulerian form, which is solved by OpenFOAM through PISO (Pressure-Implicit with Splitting of Operators) iterations:

$$\frac{\partial \phi_f}{\partial t} + \nabla \cdot (\phi_f \mathbf{u}_f) = 0 \tag{2}$$

$$\frac{\partial \rho_f \phi_f \mathbf{u}_f}{\partial t} + \nabla \cdot (\rho_f \phi_f \mathbf{u}_f \mathbf{u}_f) = -\phi_f \nabla p - \mathbf{F}_f + \nabla \cdot (\phi_f \boldsymbol{\tau}) + \phi_f \rho_f \mathbf{g} \tag{3}$$

where ϕ_f is the void fraction of a fluid cell, which is calculated as (1-ϕ_s) and ϕ_s is the solid fraction obtained from DEM; $\mathbf{u}_f$ is the fluid velocity; ρ_f is the fluid density; p denotes the pressure in the fluid cell and $\boldsymbol{\tau}$ is the stress tensor; $\mathbf{g}$ is the gravity and $\mathbf{F}_f$ is the fluid–particle interaction force.

The CFDEM code is used for calculating the fluid–particle interaction forces at a certain interval of time step, and for updating the field data simultaneously. A comprehensive introduction to fluid–particle interaction forces can be found in Zhu et al. [27]. Note that only the drag force, the pressure gradient force and the viscous force were considered in these simulations following Smuts [28] as other forces such as lift force and virtual mass force are insignificant in a slurry–particle system. Detailed formulations of the forces considered in the current simulations are available in [20].

2.2 Model implementation

The size of sand particles was fixed while the slurry particle size and cohesion energy density were varied to obtain different types of filter cake. To determine an appropriate diameter for the filtration column, a compromise must be made between the column size and the number of particles. There is also a numerical requirement: the smallest unit of the CFD mesh should be larger than the particle in the CFD–DEM code adopted for this research [29], a restriction which is not required for alternative diffusion-based methods [30]. The sand particles used in the current simulation were 3 *mm* in diameter and the diameter of the filtration column was determined to be 6 *cm*. The shortest dimension of the smallest unit of the adopted CFD mesh shown in Figure 3 was 3.75 *mm*: larger than the sand particle diameter, as required.

During the simulation, 10000 sand particles were firstly randomly generated inside the filtration column region and settled under gravity to create a sand column with a height of around 8 *cm*. Then the sand column was saturated by coupled calculation with the fluid phase until the pressure and velocity fields of the fluid phase reached steady states. After saturation, the slurry particles were inserted randomly above the sand column to simulate the homogenous slurry suspension. Under gravity and the application of a constant fluid pressure on the top boundary, the slurry particles began to settle. When the total energy of the whole system reached an extremely low value of 10^{-7} *J*, the computation was stopped. This value was chosen because when the total energy of the system is lower than 10^{-7} *J*, the particles in suspension were stationary and the porosity and the pressure drop remained constant. Figure 4 shows the model at different stages of a representative simulation.

Five size ratios between sand particles and slurry particles were considered: *D*/*d*=3, 4, 5, 6, 7, where *D* is the diameter of sand particles and *d* is the diameter of slurry particles. Based on [20], three cohesion energy densities were used: *k*=0, 100000, 300000 J/m^3, to represent cohesionless particles, slightly cohesive particles and extremely cohesive particles, respectively. In total, 15 cases were simulated as shown in Table 1. The number of slurry particles increases with *D*/*d* in order to keep the total volume of slurry particles constant across all simulations. Other input model parameters are presented in Table 2. The friction coefficient of slurry particles matches the value chosen by Smuts [28] and other parameters used are consistent with our previous work [20]. The chosen applied pressure is within the range of values typically chosen for laboratory slurry filtration tests [5,8,10].

Table 1. Summary of simulation information

Case	*D/d*	*d*(*mm*)	*k* (J/m^3)	Number of slurry particles
a	3	1	0	20000
b	3	1	100000	20000
c	3	1	300000	20000
d	4	0.75	0	47407
e	4	0.75	100000	47407
f	4	0.75	300000	47407
g	5	0.6	0	92592
h	5	0.6	100000	92592
i	5	0.6	300000	92592
j	6	0.5	0	160000
k	6	0.5	100000	160000
l	6	0.5	300000	160000
m	7	0.428	0	255093
n	7	0.428	100000	255093
o	7	0.428	300000	255093

Table 2. Input numerical parameters

	Parameter	Value or Type
Sand particle	Diameter	3 mm
	Young's modulus	70 GPa
	Particle number	10000
	Poisson's ratio	0.3
	Friction coefficient	0.3
	Restitution	0.3
	Contact model	Hertz
Slurry particle	Young's modulus	5 MPa
	Poisson's ratio	0.3
	Restitution	0.3
	Contact model	Hertz
	Friction coefficient	0.05
Fluid	Type	Newtonian
	Kinematic viscosity	1×10^{-6} m^2/s
	Density	1000 kg/m^3
Modelling parameter	Applied pressure, P_a	30 kPa
	DEM time step	1×10^{-7} s
	Coupling interval	100
	Temperature	20 °C

3. Validation

A qualitative validation was conducted in our previous work [20] by comparing the pressure filtration characteristic obtained in simulations with that of Min et al.'s experiments [31]. Though clay slurry rather than bentonite slurry was used in their experiment, both materials have similar capacity in terms of filter cake formation and support pressure transmission. Consequently, pressure transmission curves similar to the experimental ones of Min et al. were obtained in the current numerical simulations. The quantitative validation of the present simulations was conducted based on the Ergun equation, a variant of the Kozeny–Carman equation [32-33]. This empirical equation is used for predicting the fluid flow behavior through a dense particle system, i.e., the relationship between pressure drop and fluid velocity:

$$\frac{\Delta p}{\Delta L} = 150\frac{(1-\phi_c)^2 \mu V_s}{\phi_c^3 d_p^2} + 1.75\frac{(1-\phi_c)\rho_f V_s^2}{\phi_c^3 d_p} \quad (4)$$

where Δp is the pressure drop across the cake; ΔL is the thickness of the cake; V_s is the superficial velocity; μ and ρ_f are the dynamic viscosity and density of the fluid phase; d_p is the diameter of slurry particles; ϕ_c is the porosity of the filter cake. Eq. (4) was established by calibrating fitting parameters (i.e., 150 and 1.75) based on a large number of experimental data points.

Δp, ΔL, and ϕ_f were obtained under different *D*/*d* values from the numerical simulation. V_s was then calculated based on Eq. (4) and compared with the numerical superficial velocity. The porosity was calculated using the divided void fraction method, in which the exact volume fraction of the particles in each fluid cell was accurately determined [34]. Note that only the pressure drop across the external filter cake was considered in the validation. Consequently, only those cases in which external filter cake could form were used (when *k=300000 J/m*^{3}). The simulation conditions and physical properties of these cases can be found in Table 1 and Table 2. Figure 5 compares the superficial velocities obtained from numerical simulations with those predicted by Eq. (4). Overall, the simulation results agree with Kozeny–Carman; the maximum and minimum discrepancies are 11.6% for *d*=0.428 *mm* (*D*/*d*=7) and 0.2% for *d*=1 *mm* (*D*/*d*=3), respectively. The discrepancy decreases when the diameter of slurry particles increases. The discrepancies may be due to two reasons. The first reason is the semi-empirical nature of the Kozeny–Carman equation. The fitted constants in Eq. (4), i.e., 150 and 1.75, were calibrated based on a variety of experimental results. Many researchers have suggested modifications to these constants [35-36]. Furthermore, as indicated by Tien and Ramarao [37], in some cases these correlations were shown to only have an accuracy of 50%. The second reason is the validation cases used k=300000 J/m^3 so that compact filter cakes (Type I) could be generated. Hence, aggregates and inter-aggregate pores were formed inside the filter cake as shown in Figure 6. This differs from the experiments used to establish the Kozeny–Carman equation, in which cohesionless particles have normally been used.

4. Result analysis

4.1 Filter cake morphology

Figure 7 (a)~(o) shows the filter cake morphology with different combinations of D/d and k. In each sub-figure of Figure 7, the left side depicts the slurry particles and sand particles together, and the right side shows only the centroids of these particles.

4.1.1 Definitions of basic slurry filtration behaviors

Min et al. [10] identified three basic types of filter cake whose formations were dependent on D/d, namely thick filter cake (type I), a medium filter cake plus an infiltration zone (type II) and an infiltration zone without filter cake (type III). However, these classifications were based on naked-eye observations of the slurry filtration column tests; these were limited by the clarity of the fluid and could not reveal the formation mechanisms of different types of filter cake from a particulate perspective. Considering the cake morphology shown in Figure 7, three basic types of slurry filtration were defined as illustrated schematically in Figure 8: external filter cake, internal filter cake, and deep penetration. The external filter cake forms when the slurry particles or the aggregates of slurry particles are large enough to clog the void throats on the surface of the sand column so that no slurry particles could further infiltrate into the sand column. Typical external filter cakes are seen in Figure 7(a), (b), (c), (f), (i), (l) and (o). An internal filter cake forms when the slurry particles are small enough to pass through the surface layers of the sand column. The infiltrating slurry particles gradually fill the pore throats and seal the surface layers of the sand column, thereafter preventing further infiltration. In this case, a large number of slurry particles are retained in the deep layer due to the particle bridge effect [14,38] (see Figure 9) or clogging of the void throats between sand particles. The stagnation of slurry particles in soil pores may also occur because of a balance between the driving force exerted on slurry particles and the shear forces of the channel wall as the hydraulic gradient will gradually decrease in the soil pores when slurry infiltration develops. Internal filter cake always appears with either external filter cake (see Figure 7(*g*), (*k*), (*n*)) or deep penetration (see Figure 7(*j*), (*m*), (*n*)). Deep penetration happens when the slurry particles are extremely small or the cohesion between them is not strong enough to create large aggregates so that a great number of slurry particles infiltrate deeply into the sand column and eventually deposit at the bottom. Similar to internal filter cake, deep penetration also appears in conjunction with other types of filtration as shown in Figure 7(*j*), (*m*), (*n*).

4.1.2 Influences of size ratio and cohesion energy density on cake morphology

As shown in Figure 7, the influences of size ratio and cohesion energy density on the final cake morphology when the slurry suspension system becomes stable are coupled. When the slurry particles are relatively large, i.e., D/d=3, only external filter cake is formed irrespective of cohesion energy density. Slurry particles could clog the void throats on the surface of the sand column without forming aggregates. This phenomenon is in accordance with Terzaghi's filtration rule. As the diameter of slurry particles decreases, they begin to infiltrate into the voids between sand particles. Referring to Figure 7(*d*), (*e*) and (*g*), the combination of an external filter cake and an internal filter cake is found when *D*/*d*=4 in the cohesionless (k=0 J/m^3) and slightly cohesive cases (k= 100000 J/m^3) as well as in the cohesionless case (k=0 J/m^3) when *D*/*d*=5. This phenomenon happens because the slurry particles could pass through some of the void throats on the surface of the sand column and infiltrate to a certain distance as the sizes of void throats are not uniform even for uniform sand particles. In these cases, most of the slurry particles are retained on the surface of the sand column which results in the formation of an external filter cake. In the case of *D*/*d*=5, many more slurry particles infiltrate into the sand column, leading to a more substantial internal filter cake than that in the case of *D*/*d*=4 as shown in Figure 7(*d*) and (*g*). When the cohesion energy density increases, only external filter cakes are observed and large aggregates of slurry particles appear as shown in Figure 7(*f*), (*h*) and (*i*). This explains the transition from external & internal filter cake to solely external filter cake when increasing the cohesion energy density in the cases of *D*/*d*=4 and *D*/*d*=5. As the diameter of slurry particles further decreases (*D*/*d*=6 and *D*/*d*=7), the majority of slurry particles could pass through the voids in the surface layer of the sand column in the cohesionless case. A large number of slurry particles deposit at the bottom of filtration column, which corresponds to deep penetration as defined in Figure 8(*c*). However, there are still many slurry particles retained in the upper voids due to the particle bridge effect, which leads to the formation of internal filter cake as shown in Figure 7(*j*) and (*m*). Referring to Figure 7(*k*) and (*n*), when the cohesion energy density rises to 100000 J/m^3, apart from the internal filter cake and deep penetration, external filter cake is also found on the top surface of the sand column in the cases of *D*/*d*=6 and *D*/*d*=7. This indicates that aggregates large enough to clog the surface voids appear. In the extremely cohesive case when *k*=300000 J/m^3, only external filter cakes are observed. However, there is a distinct increase in the thickness of the external filter cake when *D*/*d* increases from 3 to 7, which suggests that smaller particles have the tendency to form larger aggregates and make the external cake looser (see Figure 7(*c*), (*f*), (*i*), (*l*) and (*o*)). The coupled effects of size ratio and cohesion energy density on the morphology of the filter cake can be summarized as follows:

1) Slurry particles with a large size ratio tend to fill the voids between sand particles, which could be compensated by the particle bridge and aggregation effects that are enhanced by increasing cohesion energy density. Therefore, even in the cases when the slurry particles are very small (*D*/*d*=6 and *D*/*d*=7), internal and sometimes external filter cake forms in addition to deep penetration.

2) Cohesion between the slurry particles encourages their aggregation. When the slurry particles are slightly cohesive (*k*=100000 J/m^3), the types of filter cake formed depend on the size ratio. However, when the slurry particles are extremely cohesive (*k*=300000 J/m^3), only external filter cakes form.

4.2 Pressure transmission characteristics

The morphology of the filter cake influences its porosity and permeability, which therefore affects the pressure transmission along the filtration column. The effectiveness of the filter cake can be evaluated by 'pressure drop', which is defined as the pore pressure difference across the filter cake. The value of pressure drop across the cake also indicates the effective pressure transmitted by the filter cake to the strata. According to the Kozeny–Carman equation, porosity would significantly influence the pressure drop across the filter cake. Figures 10 to 13 compare the porosity and pressure distributions at the end of the representative simulations shown in Figure 7 with those at the original state.

4.2.1 External filter cake

Figure 10 shows the typical porosity and pore pressure distribution curves of the external filter cake. At the original state prior to slurry filtration, the porosity in the region 0~0.08 *m* from the bottom of the column (*Z*) varies between 0.38~0.43. There is a transition zone where the porosity changes gradually from slurry suspension to the sand column. The distribution of porosity when an external filter cake has formed can be divided into three distinct parts: 1) sand column where $Z < 0.08$ *m*; 2) external filter cake where Z=0.08~0.1 *m*; 3) pure liquid where Z>0.1 *m*.). The obtained filter cake is thicker than that commonly observed in the infiltration column tests. The reasons may be two-fold: firstly, the slurry particles used in simulations are larger than real slurry particles to save computational cost; secondly, the slurry particles are represented by spheres, which thereby leads to a looser packing of filter cake in comparison to the experiments. The porosity within the external filter cake region decreases significantly in comparison to the original state due to the infiltration of slurry particles which fill the pores on the top surface of the sand column. A minimum local porosity of 0.32 is found in the cohesionless case ($k=0\ J/m^3$) when $D/d=3$, while in other cases the minimum local porosities vary from 0.35 to 0.38. Generally, with the same D/d, slurry particles with lower cohesion will result in an external filter cake of lower minimum local porosity. This indicates that cohesionless slurries tend to form more compact filter cakes than cohesive slurries: expected as the formation of aggregates of cohesive slurries will create inter-aggregate voids (see Figure 6). Referring to Figure 10(b), the decrease of local porosity results in an almost linear pore pressure drop within the external filter cake. The filter cake with lowest local minimum porosity (D/d=3, k=0 J/m^3) has a pore pressure drop of 10.85 kPa, which is lower than that when D/d=7, k=300000 J/m^3 due to its larger slurry particles. This observation is in accordance with the Kozeny–Carman equation which indicates that the pressure drop increases with decreasing porosity and slurry particle diameter.

4.2.2 External & internal filter cake

Figure 11 depicts the distributions of pore pressure and porosity of the external & internal filter cake. For clarity, only the boundaries of partitions of different infiltration zones for D/d=4 are marked. In the cases of D/d=4, only a few slurry particles infiltrate into the sand column (see Figure 7(d) and (e)). In these cases, the porosity distribution is similar to that of the external filter cake with the same size ratio (marked by green inverted triangles in Figure 10) but its infiltration distance is longer. Furthermore, the minimum local porosity of external & internal filter cakes formed in these cases is 0.32: lower than 0.38 for the pure external filter cake. This is expected as lower porosities are achievable in binary mixtures of packed spheres than for monosized spheres [39]. As a result, the corresponding pressure drop within the filter cake is higher than pure external filter cake, i.e., the pressure drops within the external & internal filter cakes formed in D/d=4 are 10.8 kPa and 11.9 kPa for k=0 J/m^3 and k=100000 J/m^3, respectively, which are 22.5% and 35% higher than that of the external filter cake with the same size ratio and k=300000 J/m^3 (8.8 kPa). In the cases of D/d=5 and D/d=6, the porosity distribution curves above Z=0.03 m deviate from the original state due to deeper infiltration. The porosity initially decreases as Z increases, reaching a local minimum of 0.295 at Z=0.075 m in the case of D/d=5, k=0 J/m^3 and a local minimum of 0.32 at Z=0.08 m in the case of D/d=6, k=100000 J/m^3. The low porosity prevents the remaining slurry particles from further infiltration, and thus the porosity then increases until it reaches the porosity of the pure liquid. The gradient of the pressure drop is high and nonlinear in regions where the porosity changes significantly.

4.2.3 Internal filter cake & deep penetration

As defined in Figure 8(c), deep penetration is characterized by deposition of a large amount of slurry particles at the bottom of the sand column. Hence, referring to Figure 12(a), the porosity distribution of internal filter cake & deep penetration deviates from the original state throughout the height of the filtration column. A sharp decrease of porosity is observed from Z=0.01 m to Z=0 m with the minimum porosities (0.3 in case of D/d=6, k=0 J/m^3 and 0.2 in case of D/d=7, k=0 J/m^3) occurring at the bottom. From Z=0.01 m to Z=0.08 m, the deviation gradually becomes larger due to the formation of an internal rather than an external filter cake (see Figure 7(j) and (m)). The pore pressure distribution curves also exhibit obvious differences from the cases of external or external & internal filter cakes. A large pressure drop occurs at the bottom of the column from Z=0 m to Z=0.01 m due to the low local porosity caused by particle deposition. Above this region, the pressure rises linearly to the applied pressure (30 kPa). It should be noted that particle deposition only occurs in the filtration column test. If the infiltration time is long enough, the slurry particles would eventually seal pores of the sand column and form internal or external filter cake. That's why it is still called a combination of filter cake and deep penetration from a morphology perspective. However, in real SPB tunneling, there is no boundary to retain slurry particles. In reality, deep penetration results in the continuous loss of slurry particles. Therefore, the support pressure may oscillate and the tunnel face would collapse before an effective filter cake forms. Consequently, deep penetration should be avoided in engineering practice.

4.2.4 External & internal filter cake & deep penetration

The pressure filtration behaviors of the external & internal filter cake & deep penetration are similar to the internal filter cake & deep penetration except that some slurry particles are retained on the surface of the sand column due to aggregation. As seen on Figure 13(a), the local porosity at the bottom of the column (0.35) is larger than that of the internal filter cake & deep penetration (see Figure 12). Due to the formation of external & internal filter cake around the surface of the sand column, the minimum porosity in that area (0.31) is smaller than for the internal filter cake & deep penetration presented in Figure 12. Therefore, it is more difficult for slurry particles to infiltrate deeper. The pore pressure distribution in this case is similar to that described in Section 4.2.3. The change in the slope of pore pressure distribution is less notable than that presented in Figure 12 due to the smaller change of porosity.

5. Pore structure analysis

Slurry filtration is essentially a dynamic process in which the slurry particles travel through and fill the pores between the sand particles. The pore structure of the sand changes. The slurry particles can only pass through pore 'throats' which are larger than their diameter but clog at smaller pore throats. The filtration path and number of infiltrating particles depend on the pore structure of the sand column. Therefore, it is important to understand the characteristics of pore structure evolution during the slurry infiltration process. However, extracting the void structure from 3D DEM simulation data is non-trivial as the topology of the void space emerges indirectly from the DEM output [21]. Consequently, a specific algorithm is necessary to convert the DEM data into void topology. Several have been developed including the 'maximal balls method' [40], the weighted Delaunay triangulation [18, 41, 42] and the contact-based void partitioning method [21]. Though based on different principles, these methods yield comparable results [41]. The contact-based void partitioning algorithm developed by O'Sullivan et al. [21] is adopted herein to identify the pore structure as this method can avoid both the rather subjective specification of an overlap value in the weighted Delaunay triangulation and the conversion of the DEM dataset to a 3D image format to apply the 'maximal balls method' [21].

The basic principle of this approach is illustrated in Figure 14. A set of tetrahedra are generated using the Delaunay triangulation based on the contact points. The generated tetrahedral cells are classified into solid cells if all four vertexes belong to the same particle, or void cells otherwise. The void cells whose vertexes are not in a closed loop of three or four contacting particles are merged to form a larger void cell, while the face of void cells with contacts between particles forming a closed loop is taken as a constriction. The constriction size is defined as the diameter of the largest sphere that can fit in the constriction (see Figure 14(b)).

More details about the algorithm are provided in O'Sullivan et al. [21]. The constriction size distribution (CSD) curve is a direct measurement of the pore structure and dimension of infiltration path. Consequently, this section uses CSD curves to show the spatial distribution and evolution of the pore structure of the filter cake in the slurry filtration process.

5.1 CSD of the sand column

Figure 15 compares the CSD of the sand column at the start of the test and the PSDs (particle size distributions) of the slurry particles in the simulations. The constriction sizes of the sand column range from $0.155D$ (in agreement with the theoretical minimum diameter) to $0.4D$, where D is the diameter of the sand particles. When the slurry particles are larger than 89% of the constrictions (D/d=3), no slurry particles could infiltrate into the sand column, resulting in the formation of external filter cake. For slurry particles that are larger than 69% of the constrictions (when D/d=4), a few particles could infiltrate into the top surface of the sand column. These particles clog the pore space and prevent further infiltration. Therefore, the remaining particles deposit on top of the sand column, forming an external & internal filter cake. The internal filter cake is much more notable and slurry particles infiltrate deeper when the size of slurry particles is close to D_{c50} (the median constriction size) in the case of D/d=5 as shown in Figure 15 and Figure 7(g). When the particle size is smaller than D_{c50}, a large number of slurry particles infiltrate into the sand column and deep penetration occurs. In this case, external filter cake is barely formed. Based on the above observations, $d=D_{c50}$ can be regarded as an important indicator for assessing the slurry filtration process. In particular, $d=D_{c50}$ is defined as the criterion separating slight infiltration from deep penetration.

5.2 Evolution of CSD during the filtration process

In order to explore the spatial characteristics of pore structure inside different types of filter cakes, the filtration columns are split into four partitions whose locations are shown in Figure 16. The upper two partitions (① and ②) are thinner than the bottom two because a large number of slurry particles will be trapped in the upper partitions and variation of porosity is most significant here. The CSD of each partition for different simulations is shown in Figure 16. For Case c (Figure 16(a)), the slurry particles are larger than 89% of the constrictions in the sand column. Very few slurry particles infiltrate into the sand column. Therefore, the CSDs of partitions ②, ③, ④ are very close to the CSD of the sand column. The CSD of partition ① deviates significantly from the CSD of the sand column with a minimum constriction size of 0.065d and a D_{c50} of 0.13d. This compact filter cake prevents the slurry particles from further infiltration. In the cases of external & internal filter cake or deep penetration (see Figure 16(b), (c), (d)), with the slurry particles penetrating into the voids, the CSDs of partitions ②, ③, ④ begin to deviate from the CSD of the sand column and gradually approach the CSD of partition ①. The CSDs of partitions of simulations with more infiltrating slurry particles deviate more notably from the CSD of the sand column and approach that of partition ① with a smaller D_{c50}. Figure 17 illustrates the distribution of D_{c50} inside the filtration column, which shows a clear correlation between D_{c50} and the slurry filtration state. When no slurry particles infiltrate into the sand column, the differences between the D_{c50} of partition ① and other partitions are comparatively large. However, as more slurry particles infiltrate into the sand column, a more uniform distribution of D_{c50} along the filtration column is observed as the filtration column itself has become a more homogenous system.

The CSDs of four typical types of filter cake at different instants during the simulation are calculated to investigate the evolution of the pore structure during the slurry filtration process. In the case of external filter cake (Figure 18(*a*)), the CSDs during the filtration process are close to the original state. The CSD after filtration for 0.1 *s* deviates slightly from the original sand column and remains constant after 0.2 *s*. This is because some slurry particles infiltrate into the top surface of the sand column and seal the infiltration channel. The remaining slurry particles deposit gradually on top of the sand column without further infiltration after 0.1 *s*. In the cases of external & internal filter cake (Figures 18(*b*), (*c*), (*d*)), the overall evolution trends at different instants are similar: the constriction size decreases notably at 0.1 *s*-0.2 *s* and remains approximately constant from 0.3 *s*-0.7 *s*. The slight differences of CSDs after 0.3 *s* result from slight movements of slurry particles inside the sand column. Larger slurry particles result in slower and more gradual infiltration as the larger particles are more likely to become trapped between sand particles and need more time to infiltrate. Therefore, the CSDs after slurry filtration deviate more notably from the original state as the size of slurry particles increases. The difference in CSD between slurry filtration for 0.1 *s* and the subsequent filtration instants increases with increasing slurry particle size as it is easier for smaller slurry particles to infiltrate into the sand column. The filtration seals the pores between sand particles and prevents the remaining particles from infiltration.

Figure 19 shows the evolution of D_{c50} at different instants for the selected four simulations. D_{c50} decreases with decreasing size of slurry particles. D_{c50} decreases sharply initially due to slurry infiltration and becomes approximately stable after a certain period. The time for D_{c50} to reach stable values increases as the size of slurry particles decreases due to longer infiltration path. The time needed for D_{c50} of Case c to stabilize is 0.1*s*, while it takes 0.5 *s*, 0.6 *s* and 0.6 *s*, respectively, for D_{c50} of Cases d, g and k to become stable.

5.3 Correlation between D_{c50} and pressure drop

D_{c50} of four partitions of the external filter cake and external & internal filter cake and the corresponding pressure drop gradients across the partitions are plotted in Figure 20. The other two types of filter cake are considered to be ineffective for pressure transmission, and thus are not considered here. The normalized $\Delta P / \Delta L$ (pressure drop gradient) in Figure 20 is defined as the pressure drop gradient across the specific partition with a thickness of ΔL divided by the pressure drop gradient across the entire filtration column, and *d* is the diameter of slurry particles. Power law correlations between D_{c50} and the normalized $\Delta P / \Delta L$ of these two types of filter cake can be established: for external filter cake, $\frac{\Delta P}{\Delta L} = 2.32e^{-4.43(\frac{D_{c50}}{d})} + 0.67$ with R^2=0.95; for external & internal filter cake, $\frac{\Delta P}{\Delta L} = 1832.58e^{-34.32(\frac{D_{c50}}{d})} + 0.70$ with R^2=0.92. There is obvious deviation between the two curves when D_{c50}/d is smaller than 0.2, i.e., with the same D_{c50}/d, the external & internal filter cake tends to have higher pressure drop gradient than the external filter cake as the former yields a smaller porosity than the latter. The equations also indicate that when D_{c50}/d is greater than 0.4, the influence of D_{c50}/d on the pressure transmission is insignificant. Furthermore, these equations relate the micro-scale pore structure characteristics to the macro-scale pressure filtration performance of the filter cake quantitatively, which may be useful for predicting the pressure filtration performance of filter cake by directly comparing the characteristic pore size of the sand and characteristic size of the slurry particle from a micro-perspective.

6. Conclusions

In this paper, a series of coupled CFD–DEM simulations on slurry filtration column tests were carried out to investigate the micro-mechanism underlying the slurry filtration phenomenon. The key observations are as follows:

(1) The size ratio between sand and slurry particles and cohesiveness of slurry particles have a coupled effect on the formation of filter cake. The larger the size ratio and the smaller the cohesion, the easier it is for slurry particles to infiltrate into the voids. Under different combinations of size ratio and cohesion values, four types of filter cake could be identified: *(i)* external filter cake, *(ii)* external & internal filter cake, *(iii)* internal filter cake & deep penetration and *(iv)* external & internal filter cake & deep penetration. These types of filter cake have distinct infiltration depths and slurry sedimentation characteristics.

(2) The porosity and pore pressure distributions show that the external & internal filter cake is the most effective for face support pressure transmission, followed by the pure external filter cake. In cases with deep penetration, a large amount of slurry particles deposit at the bottom of the filtration column, leading to a high pressure drop and a low porosity at the bottom. This is unfavorable in engineering practice as a large amount of slurry will be lost at the tunnel face, inducing the oscillation of supporting pressure.

(3) Analysis of the constriction size distribution (CSD) suggests that the CSD of the sand column changes dynamically during the slurry infiltration process. The constriction sizes decrease gradually as slurry particles infiltrate continuously until a stable state is reached. The formerly infiltrating particles seal the voids between sand particles, which prevents the remaining particles from further infiltration. As a result, the pore structure of the sand column is not homogeneous but varies along its height.

(4) The infiltration properties are closely related to the median constriction size, D_{c50}. The degree of infiltration decreases as the ratio between slurry particle size and D_{c50} increases. When the size of slurry particle is smaller than D_{c50}, a large number of slurry particles will infiltrate into the sand column and deposit at the bottom, i.e., deep penetration. Power law relationships were established between D_{c50} and pressure drop gradient within both external and external & internal filter cakes, which could be used for predicting the pressure transmission performance of the filter cake by comparing the size of slurry particle and the size of pore structure directly from a micro-scale perspective.

The aforementioned observations contribute to our understanding of the fundamental mechanism of the slurry filtration process and give insight into tunnel face stability analysis when considering slurry infiltration. The influence of cohesion energy density on the formation of a filter cake is significant. However, these values were selected empirically in the current study. Future efforts will be devoted to revealing the relationship between the cohesion energy density and the two most important macro-mechanical properties of slurry suspensions, viscosity and shear strength, so that the micro-scale mechanisms and macro-scale behavior can be bridged. Furthermore, polydisperse gradings for both slurry and sand particles also need to be implemented in the future.

Acknowledgements

The research was supported by the National Natural Science Foundation of China [grant number 41877227 & 51509186].

References

[1] Fritz, P., Hermanns, S. R., Heinz, A., 2002. Modified Bentonite Slurries for Slurry Shields in Highly Permeable Soils. In: 4th International Symposium Geotechnical Aspects of Underground Construction in Soft Ground.

[2] Fritz, P., 2007. Additives for slurry shields in highly permeable ground. Rock Mechanics and Rock Engineering. 40(1), 81-95.

[3] Axelsson, M., Gustafson, G., Fransson, Å., 2009. Stop mechanism for cementitious grouts at different water-to-cement ratios. Tunnelling and Underground Space Technology. 24, 390-397.

[4] Talmon, A.M., Mastbergen, D.R., Huisman, M., 2013. Invasion of pressurized clay suspensions into granular soil. Journal of Porous Media. 16(4), 351-365.

[5] Yin, X.S., Chen, R.P., Li, Y.C., Qi, S., 2016. A column system for modeling bentonite slurry infiltration in sands. Journal of Zhejiang University-SCIENCE A (Applied Physics & Engineering). 17(10), 818-827.

[6] Saada, Z., Canou, J., Dormieux, L., Dupla, J., 2006. Evaluation of elementary filtration properties of a cement grout injected in a sand. Canadian Geotechnical Journal. 43, 1273-1289.

[7] Mohtar, C., Yoon, J., EI-Khattab, M., 2015. Experimental study on penetration of bentonite ground through granular soils. Canadian Geotechnical Journal. 52, 1850-1860.

[8] Xu, T., Bezuijen, A., 2019. Pressure infiltration characteristics of bentonite slurry. Géotechnique. 69(4), 364-368.

[9] Zhou, Z.L., Du, X.M., Wang, S.Y., Xin, C., Chen, L., 2019. Micromechanism of the diffusion of cement-based grouts in porous media under two hydraulic operating conditions: constant flow rate and constant pressure. Acta Geotechnica. 14, 825-841.

[10] Min, F.L., Zhu, W., Han, X.R., 2013. Filter cake formation for slurry shield tunneling in highly permeable sand. Tunnelling and Underground Space Technology. 38, 423-430.

[11] Terzaghi, K., 1922. Der Grundbruch an Stauwerken und Seine (The failure of dams by piping and its prevention). Die Wasserkraft, 17, 445–449.

[12] Bertram, G.E., 1940. An experimental investigation of protective filters. In: Soil Mechanics Series No.7 Cambridge MA. Graduate School of Engineering.

[13] Sherard, J.L., Dunnigan, L.P., 1989. Critical filters for impervious soils. Journal of Geotechnical and Geoenvironmental Engineering. 115(6), 927-947.

[14] Taylor, H., 2017. Assessing the potential for suffusion in sands using x-ray micro-CT images. PhD Thesis. Imperial College London. The United Kingdom.

[15] Sherard, J.L., Dunnigan, L.P., Talbot, J.R., 1984. Basic properties of sand and gravel filters. Journal of Geotechnical and Geoenvironmental Engineering. 110(6), 684-700.

[16] Foster, M., Fell, R., 2001. Assessing embankment dam filters that do not satisfy design criteria. Journal of Geotechnical and Geoenvironmental Engineering. 127(5), 398-407.

[17] Kenney, T.C., Chahal, R., Chiu, E., Ofoegbu, G.I., Omange, G.N., Ume, C.A., 1985. Controlling constriction sizes of granular filters. Canadian Geotechnical Journal. 22(1), 32–43.

[18] Shire, T., O'Sullivan, C., 2016. Constriction size distributions of granular filters: a numerical study. Géotechnique. 66(10), 826-839.

[19] Shire, T., O'Sullivan, C., 2017. A network model to assess base-filter combinations. Computers and Geotechnics. 84, 117-128.

[20] Zhang, Z.X., Yin, T., Huang, X., Dias, D., 2019. Slurry filtration process and filter cake formation during slurry shield tunnelling: Insight from coupled CFD–DEM simulations of slurry filtration column test. Tunnelling and Underground Space Technology. 87, 64-77.

[21] O'Sullivan, C., Bluthe, K., Sejpar, K., Shire, T., Cheung L.Y.G., 2015. Contact based void partitioning to assess filtration properties in DEM simulations. Computers and Geotechnics. 64, 120-131.

[22] Kloss, C., Goniva, C., Hager, A., Amberger, S., Pirker, S., 2012. Models, algorithms and validation for opensource DEM and CFD–DEM. Progress in Computational Fluid Dynamics, an International Journal. 12(2–3), 140-152.

[23] Kloss, C., Goniva, C., Hager, A., Pirker, S., 2010. A new open source CFD–DEM Perspective. Proceedings of 5th OpenFOAM Workshop.

[24] Cundall, C.T., Strack, O.D.L., 1979. A discrete numerical model for granular assemblies. Géotechnique. 29, 47-65.

[25] Johnson, K.L., Kendall, K., Roberts, A.D., 1971. Surface energy and the contact of elastic solids. Proceedings of The Royal Society A: Mathematical Physical and Engineering Sciences. 324(1558), 301-313.

[26] Kloss, C., 2018. LIGGGHTS Manual. www.liggghts.com, 330-331.

[27] Zhu, H.P., Zhou, Z.Y., Yang, R.Y., Yu, A.B., 2007. Discrete particle simulation of particulate system: Theoretical developments. Chemical Engineering Science. 62, 3378-3396.

[28] Smuts, E., 2015. A methodology for coupled CFD–DEM modelling of particulate suspension rheology. PhD Thesis. University of Cape Town. South Africa.

[29] Peng, Z.B., Doroodchi, E., Luo, C.M., Moghtaderi, B., 2014. Influence of void fraction calculation on fidelity of CFD–DEM simulation of gas-solid bubbling fluidized beds. Particle Technology and Fluidization. 60(6), 2000-2018.

[30] Xiao, H., Sun, J., 2011. Algorithms in a robust hybrid CFD-DEM solver for particle-laden flows. Communications in Computational Physics. 9, 297-323.

[31] Min F.L., Zhu W., Wei D.W., Xia S.Q., 2013. Change of pore water pressure in soil as filter cakes formed on excavation face in slurry shield (In Chinese). Chinese Journal of Geotechnical Engineering, 35(4), 722-727.

[32] Ergun, S., 1952. Fluid flow through packed columns. Chemical Engineering Progress. 48, 89-94.

[33] Eichholz, C., Nirschl, H., Chen, F., Hatton, T.A., 2012. DEM-Simulation of the magnetic field enhanced cake filtration. AIChE Journal. 58(12), 3633-3644.

[34] Zhao, J., Shan, T., 2013. Coupled CFD-DEM simulation of fluid-particle interaction in geomechanics. Powder Technology. 239, 248-258.

[35] Macdonald, I.F., EI-Sayed, M.S., Mow, K., Dullien, F.A.L., 1979. Flow through porous media-the Ergun equation revisited. Industrial and Engineering Chemistry Fundamentals. 18,199-208.

[36] Meyer, B.A., Smith, D.W., 1985. Flow through porous media: comparisons of consolidated and unconsolidated materials. Industrial and Engineering Chemistry Fundamentals. 24, 360-368.

[37] Tien, C., Ramarao, V., 2013. Can filter cake porosity be estimated based on the Kozeny–Carman equation? Powder Technology. 237, 233-240.

[38] Valdes, J.R., Santamarina, J.C., 2008. Clogging: bridge formation and vibration-based destabilization. Canadian Geotechnical Journal. 45, 177-184.

[39] Dias, R.P., Teixeira, J.A., Mota, M.G., Yelshin, A.I., 2004. Particulate binary mixtures: dependence of packing porosity on particle size ratio. Industrial & Engineering Chemistry Research. 43(24), 7912-7919.

[40] Dong, H., Blunt, M.J., 2009. Pore-network extraction from micro-computerized-tomography images. Physical Review E. 80(3), 036307-1-036307-11

[41] Shire T., O'Sullivan C., Taylor H., Sim W., 2016. Measurement of constriction size distributions using three grainscale methods. Proceedings of 8th International Conference on Scour and Erosion. 1067-1073.

[42] Reboul, N., Vincens, E., Cambou, B., 2008. A statistical analysis of void size distribution in a simulated narrowly graded packing of spheres. Granular Matter. 10(6), 457-468.

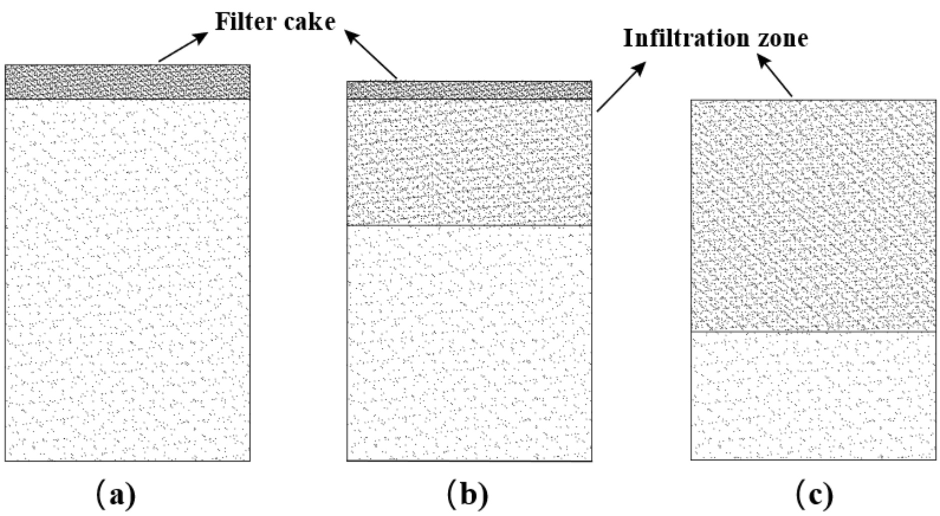

Figure 1. Three types of filter cake formation: (a) I: compact filter cake; (b) II: filter cake plus an infiltration zone; (c) III: infiltration zone without filter cake (adapted from [10])

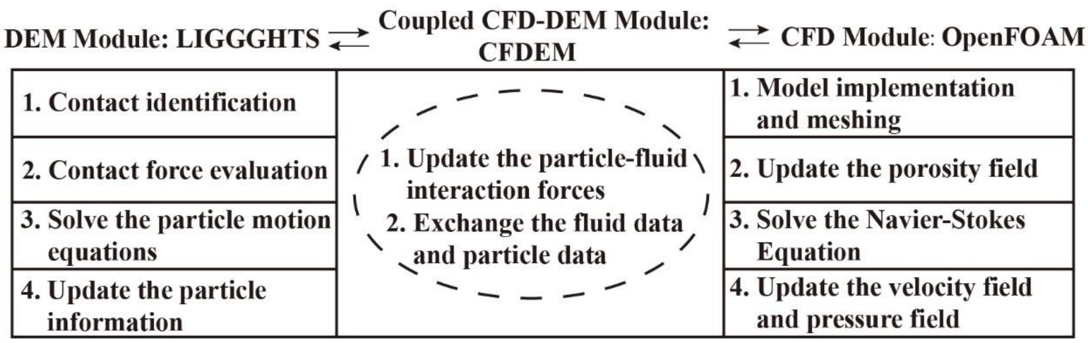

Figure 2. The coupling process of CFD and DEM

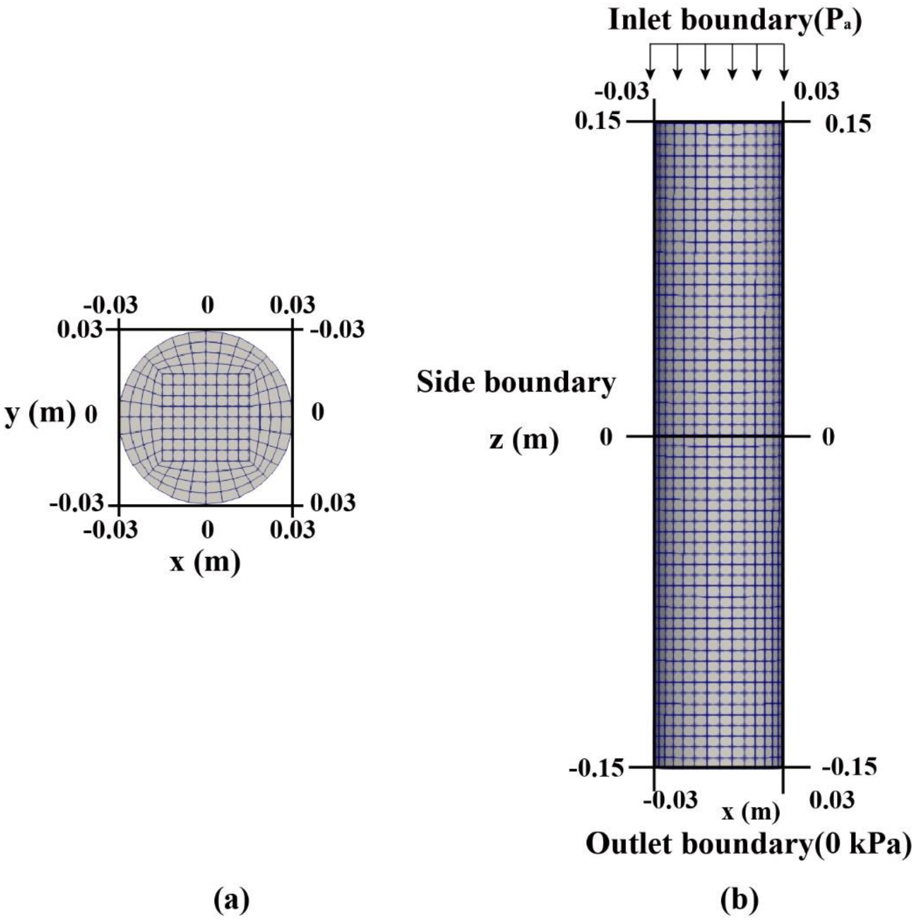

Figure 3. The mesh used in the current simulations: (a) plan view; (b) front view

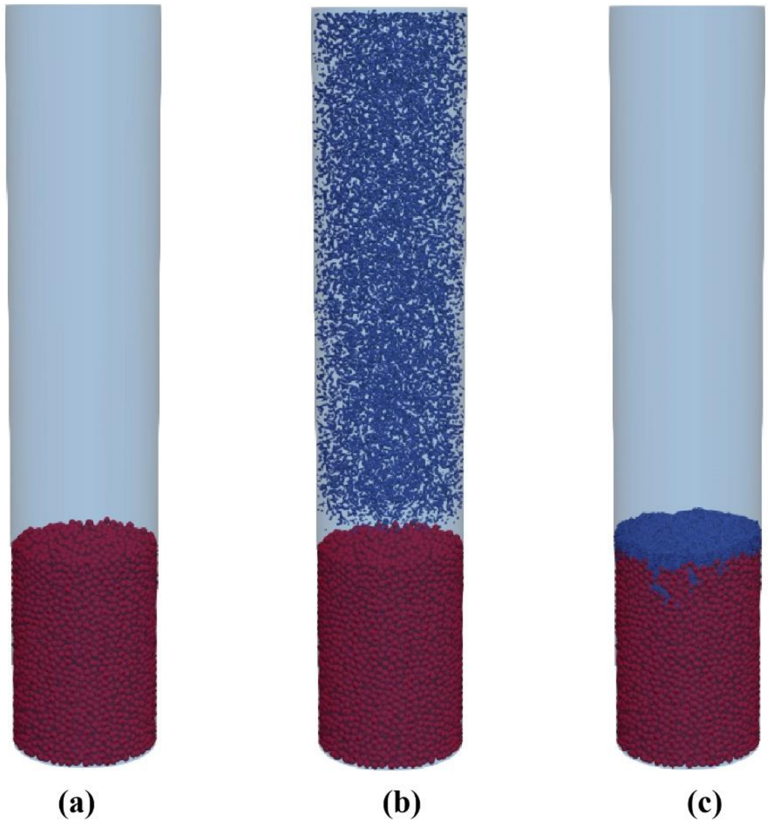

Figure 4. The modeling of the slurry column test (red represents sand grains, blue indicates slurry particles) at: (a) Sand column generation; (b) Insertion of slurry particles; (c) Filter cake formation

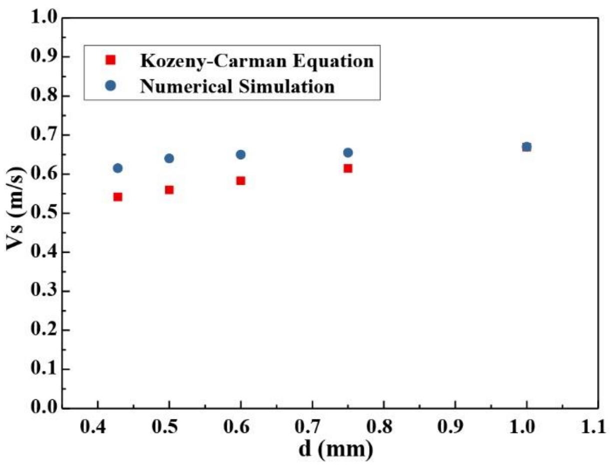

Figure 5. Comparing the numerically obtained relationship between superficial velocity and d with that predicted by Kozeny–Carman equation (in all cases, k=300000 J/m^3, P_a=30 kPa)

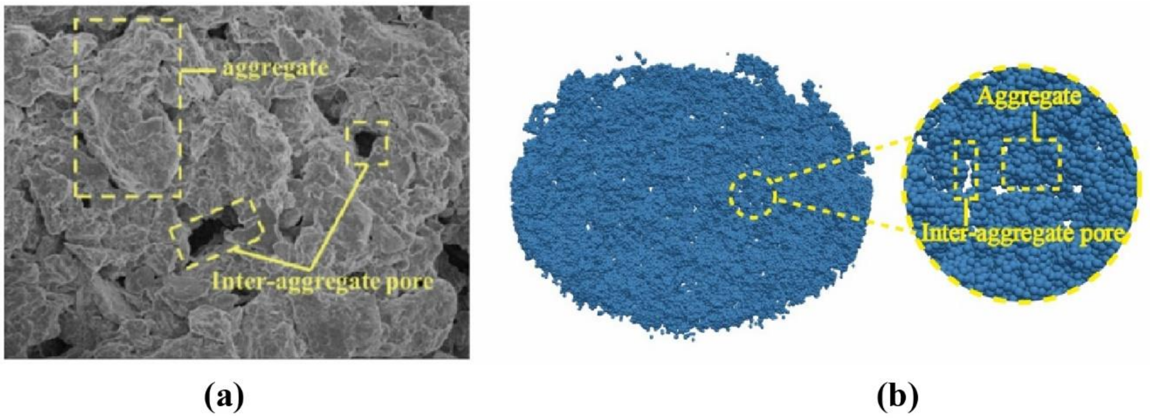

Figure 6. Aggregates of slurry particles and inter-aggregate pores forming due to cohesion inside the filter cake: (a) SEM image [36] (b) Coupled CFD–DEM simulation [19]

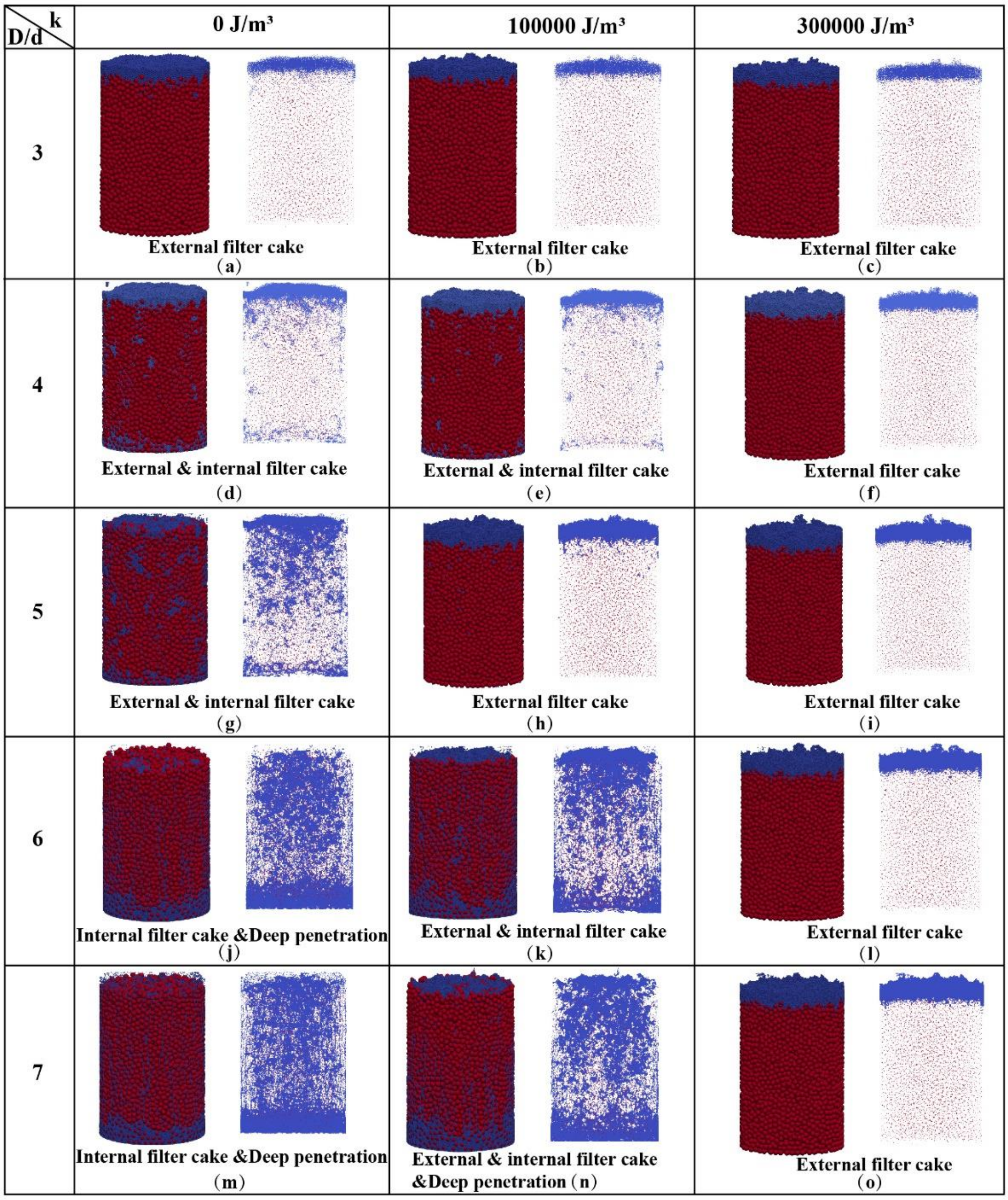

Figure 7. Illustrations of cake morphology with different combinations of *D*/*d* and cohesion energy density

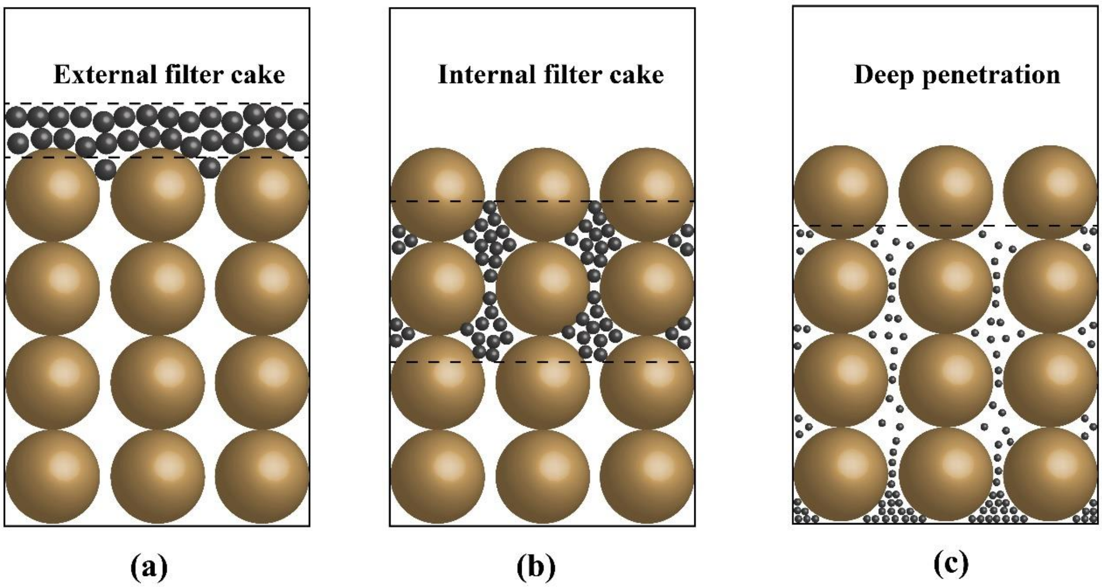

Figure 8. Schematic of different types of slurry filtration behavior

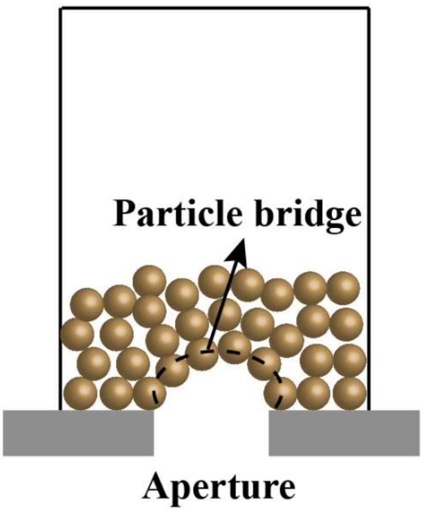

Figure 9. Particle bridge effect due to aggregation (adapted from [14])

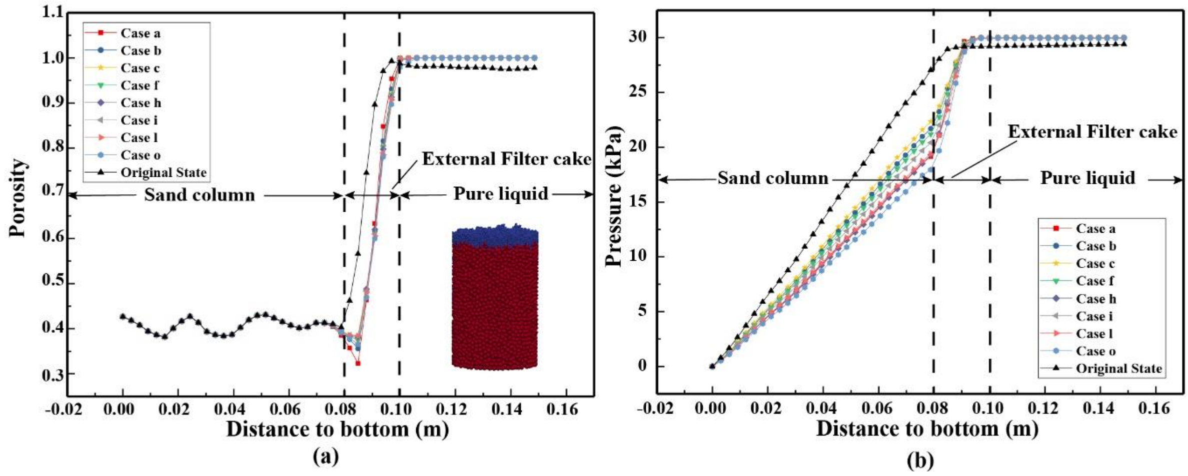

Figure 10. Comparing the (a) porosity and (b) pore pressure distributions at the end of representative simulations of external filter cake with those at the original state

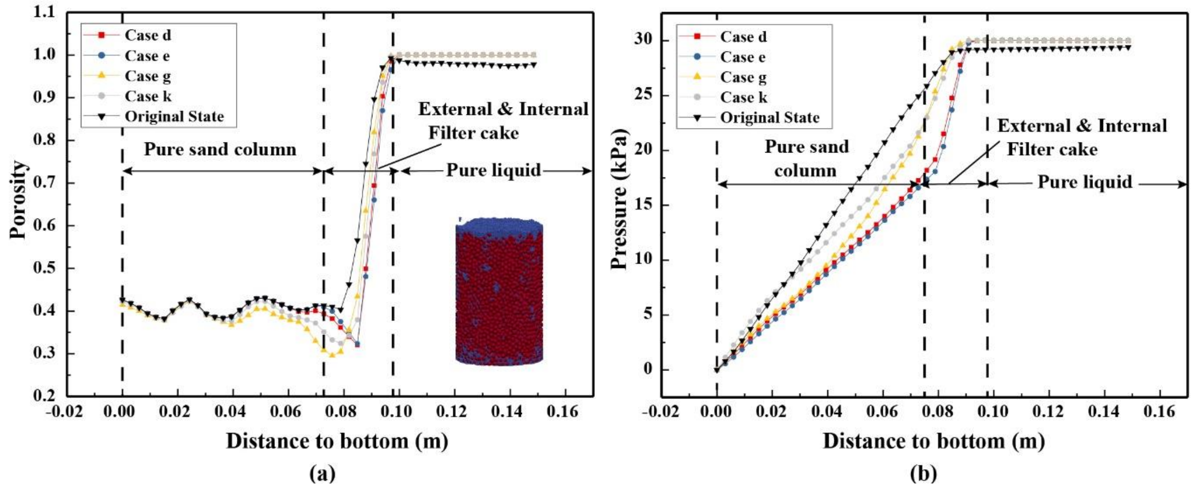

Figure 11. Comparing the (a) porosity and (b) pressure distributions at the end of representative simulations of external & internal filter cake with those at the original state

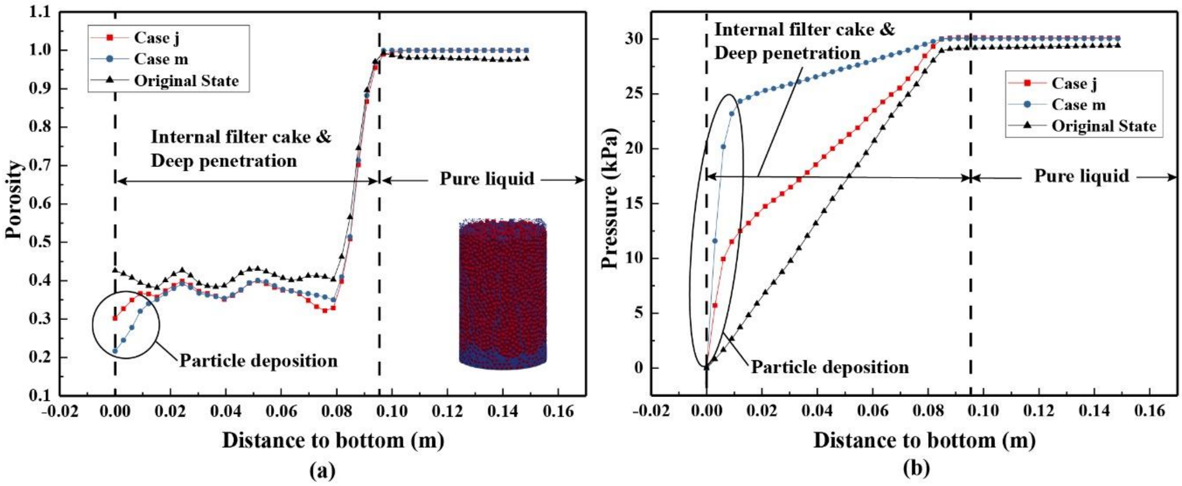

Figure 12. Comparing the (a) porosity and (b) pore pressure distributions at the end of representative simulations of internal filter cake & deep penetration with those at the original state

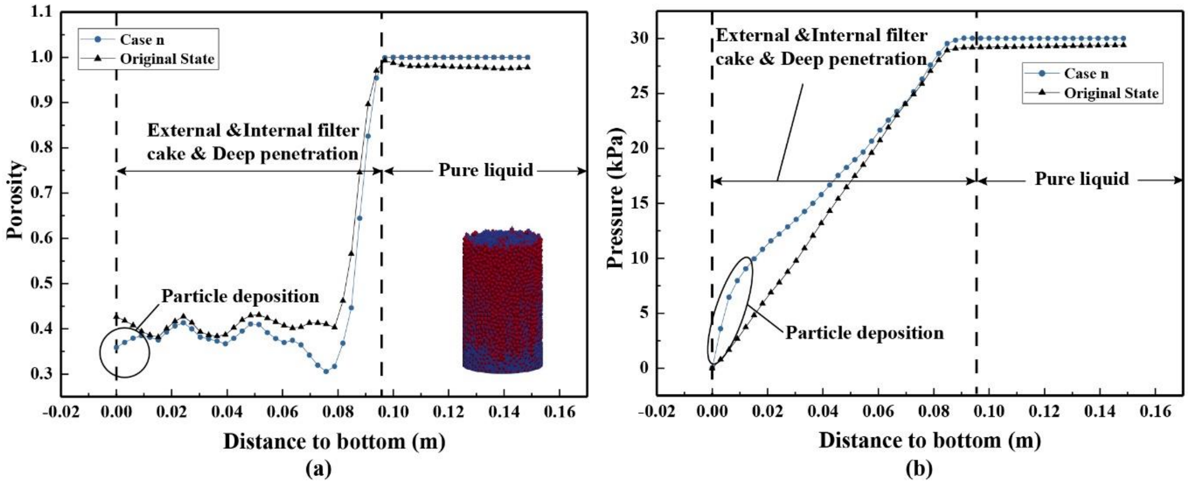

Figure 13. Comparing the (a) porosity and (b) pore pressure distributions at the end of representative simulations of external & internal filter cake & deep penetration with those at the original state

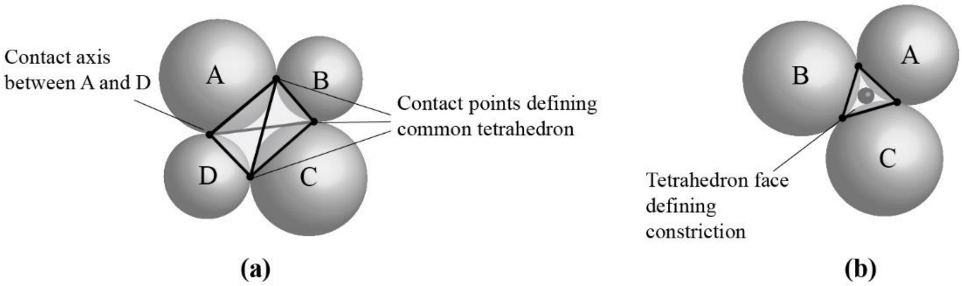

Figure 14. Identification of constriction (a) Defining a particle void in contact-based void partitioning (b) Defining the constriction size of the void in contact-based void partitioning [20]

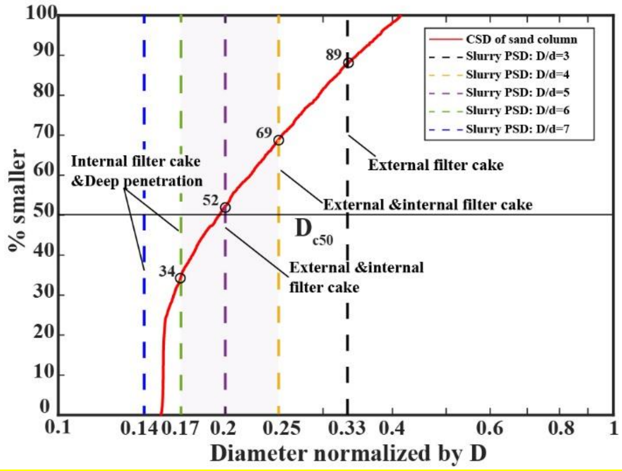

Figure 15. The CSD of the sand column and PSDs of slurry particles normalized by the diameter of sand particles (k=0 J/m^3)

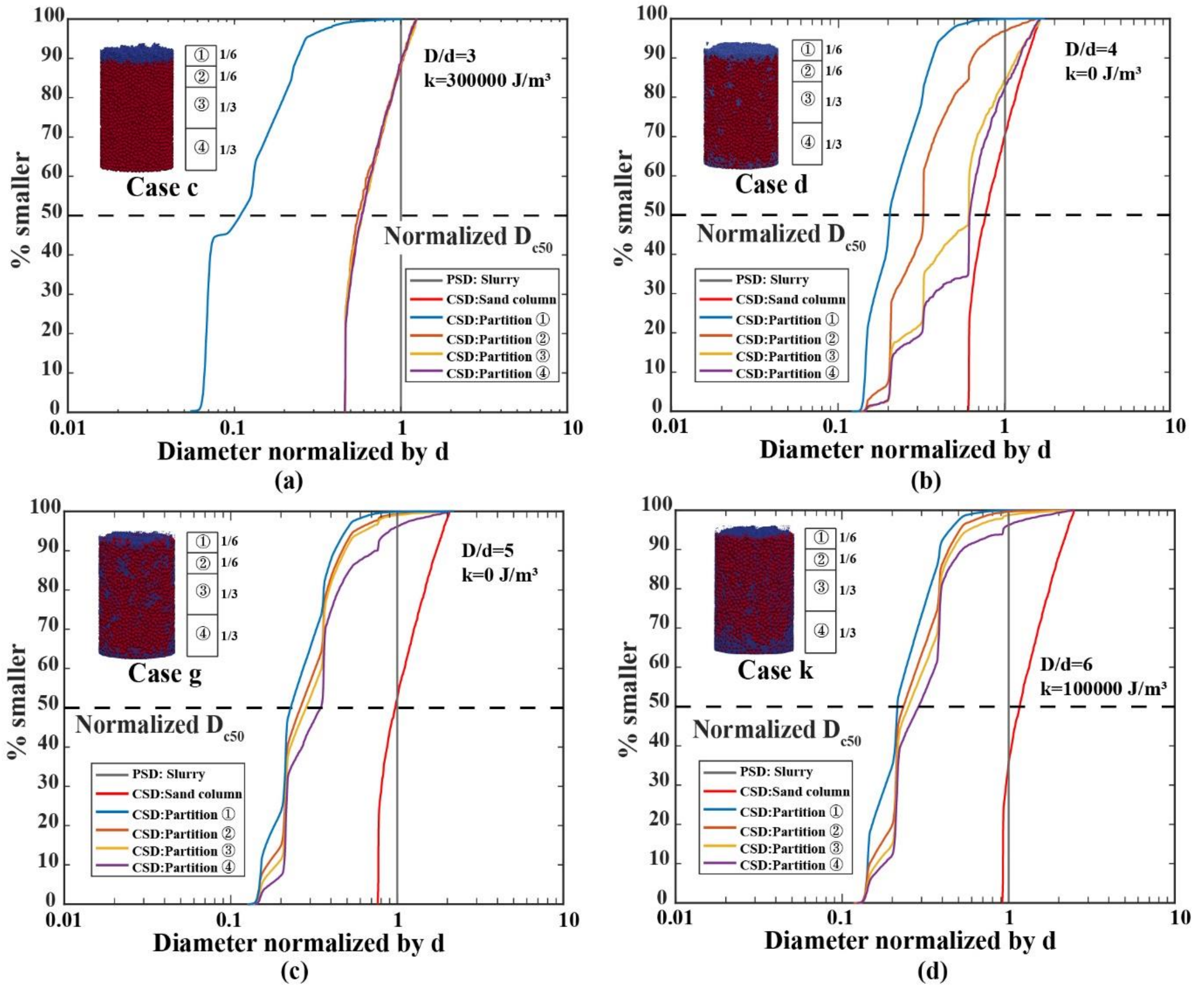

Figure 16. Spatial variation of CSDs normalized by slurry particle diameter for different types of filter cake

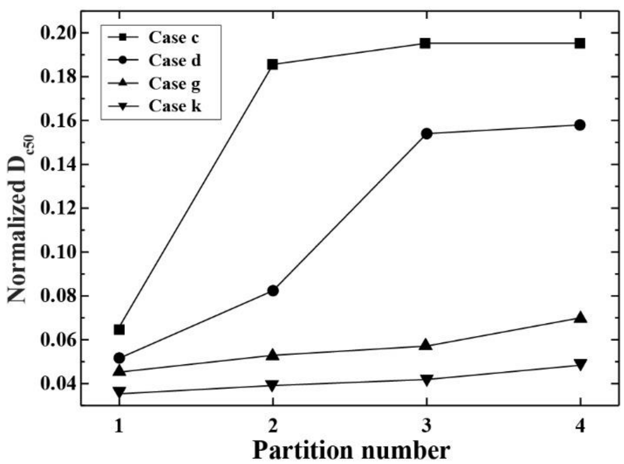

Figure 17. Distributions of D_{c50} inside different types of filter cake

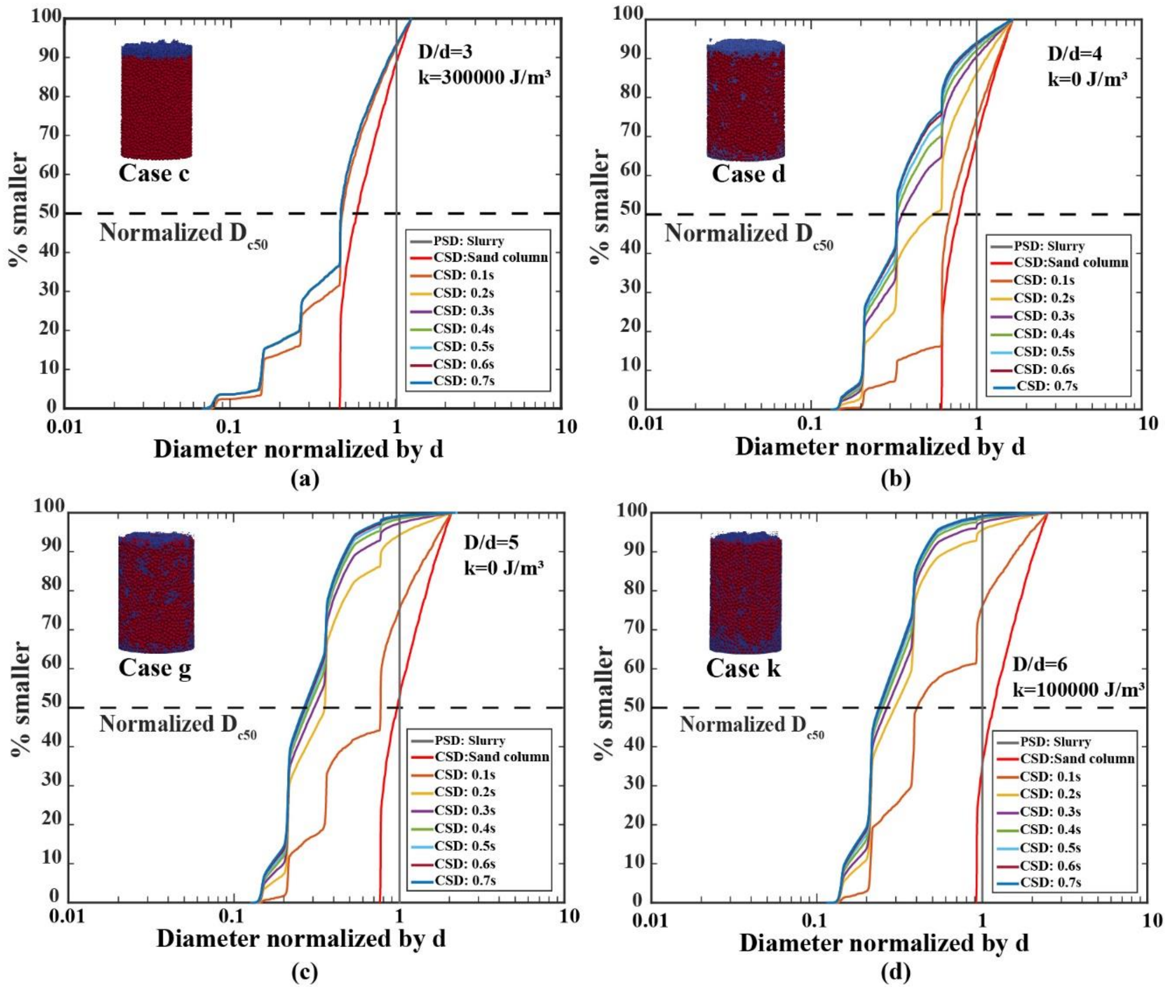

Figure 18. CSD evolutions at different instants

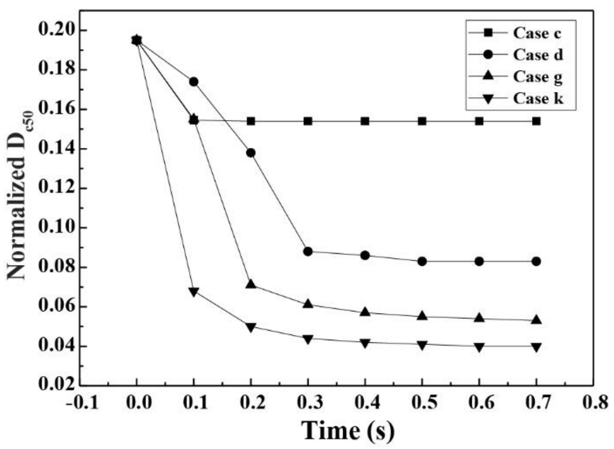

Figure 19. D_{c50} evolutions at different instants

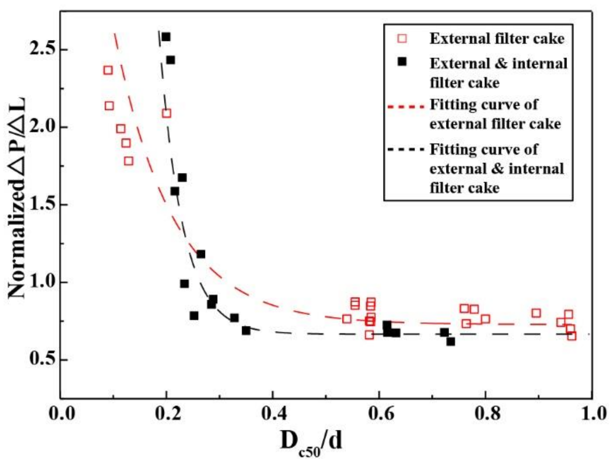

Figure 20. Correlations between D_{c50} and normalized pressure drop gradient

Author Statement

Tong Yin: Data curation, analyses, figure preparation, writing

Zixin Zhang: Supervision and funding support

Xin Huang: Conceptualization, methodology, writing

Thomas Shire: Reviewing and editing

Kevin J. Hanley: Reviewing and editing